Effect of high-compliant porosity on variations of P- and S-wave velocities in dry and saturated rocks: comparison between theory and experiment

V.Yu. Zaitsev and P. Sas[1]

Institute of Applied Physics RAS, Nizhny Novgorod, 603950, Russia
[1] Catholic University of Leuven, Leuven, 3000, Belgium

An effective medium model recently developed by the present authors is applied for interpretation of known experimental data on pressure dependencies of elastic wave velocities in dry and saturated rocks in order to elucidate the effect of the highly compliant fraction of the porosity. Our approach has allowed the determination of essential features of soft defects in terms of their shear and normal compliances. For dry defects, we found that the ratio of the normal to shear compliance may be as high as 5–7, in contrast to the range 0.8–2.2 expected for such widely used defect models as Hertz-Mindlin contacts or elliptical cracks. This high normal compliance of the real defects results in strong decrease of Poisson's ratio of the rock down to negative values. In the paper we consider an example of dry sandstone exhibiting negative Poisson's ratio. For saturated samples, we found that the normal compliance of the defects becomes smaller than the shear one (typically 1.5–3 times). From the point of view of the role of "global" (in the sense of Biot) and local (squirt) fluid flows, the performed examination indicates strong domination of the squirt mechanism including the cases, for which a third, unidentified dispersion mechanism was earlier supposed.

1. Introduction

Ample understanding of the relation between the rock microstructure and characteristics of seismic waves is one of key points for both general seismic wave modeling and interpretation in exploration seismology. A vast amount of pertinent publications relate to modeling of the wave dispersion in a wide sense, that is the velocity dependence on the frequency, external pressure, fluid saturation, microstructural features of rocks, first of all effect of pores, cracks and intergrain contacts (e.g. [1] and refs. herein). The intrinsic compliance of dry defects and their fluid saturation are crucial factors determining the elastic wave dispersion. In modeling the role of saturation one main concept originates from Biot's models accounting for the large-scale motion of the saturating fluid relative to the solid phase [2, 3]. Another important concept considers the small-scale fluid flows at grain contacts or inside cracks, that is the "squirt flow" concept [4–8]. Comparison with experiments indicates that in high-porosity materials (like artificial packings of glass beads) the Biot mechanism is rather essential [1]. In contrast, the data on elastic wave velocities in real rocks often indicate that the squirt mechanism dominates, although for some cases the observed dispersion apparently could be satisfactorily described neither by the global nor by the squirt flow mechanisms [9].

Below we shall apply a recently proposed effective medium model [10] to interpretation of experimental data obtained by different authors for pressure dependencies of P- and S-wave velocities in rocks. We shall compare and elucidate the role of the high-compliant porosity for both dry and saturated samples. The goal of the study is to determine properties of the high-compliance (crack-like) fraction porosity in terms of the normal- and shear- compliance of the crack-like defects. The approach [10] may be characterized as semi-phenomenological, since, at the microstructural level, the defect parameters are introduced phenomenologically, and then the resultant macroscopic properties of the medium are derived by consistent micromechanical analysis. An analogous energy-balance approach was used, for example, in the models of crack-containing solids [11–

13]. However, in this modeling the authors used concrete models of defects, in particular, the model of elliptical cracks, whereas the form of real cracks is often rather far from elliptical [14]. For the present consideration it is important that particular fracture models normally imply a rather limited variability of the ratio of the normal to shear compliance of defects. For example, for dry elliptical cracks this ratio is $(1+\gamma)(2-\gamma) \sim 2$ for most solids, where γ is Poisson's ratio for the host rock [10]. Therefore, in the whole physically allowable range of Poisson's ratio $0 < \gamma < 0.5$ for the solid matrix, the ratio of the normal to shear compliances of defects remains close to two for dry crack-like defects. Certainly, presence of a saturating fluid reduces this ratio, since the fluid decreases the crack compressibility. From this point of view, in the model to be used below the phenomenological introduction of the compliance parameters of the defects allows us to avoid the initial limitations on the normal-to-shear compliance ratio. Then by the comparison with experimental data we determine the ratio of the compliances for real defects. It will be shown that the determined ratios may significantly differ from the predictions based on conventional models such as elliptical cracks or Hertz-Mindlin contacts [15]. Note that a similar approach based on effective compliance (or stiffness) coefficients was used earlier for characterization of contacts in granular solids [16]. To this end, the known model by Digby [17] was reformulated in [16] in terms of phenomenological (non-predetermined) parameters of normal and shear stiffness of the contacts. For layered inhomogeneous rocks and solids containing planar compliant discontinuity-like fractures similar parameters of compliance were used in [18–21] for consideration of the induced anisotropy of the material or for determining the parameters of compliance of individual discontinuities from experimental data [22]. In this context, model [10] combines the description of the defects in terms of the effective compliance parameters with the energy approach and statistical averaging over arbitrary orientations of the defects like in the aforementioned models of crack-containing rocks.

As an interesting by-pass product of the performed examination, we have found an instructive example of a dry rock (sandstone) exhibiting pronounced negative Poisson's ratio at lower confining pressures. Note that for essentially anisotropic materials the possibility of negative effective Poisson's ratio is well known [23]. In paper [24] it is pointed out that presence of cracks with zero tangential compliance may result in negative Poisson's ratio of the crack-containing material. Below an interpretation will be given based on model [10] how negative Poisson's ratio may be observed in materials containing isotropically-oriented cracks with non-zero tangential and normal compliances.

In the context of the effect of fluid saturation, the performed examination of the experimental data indicates strong domination of the squirt (local-flow) mechanism in the pressure-dependent part of the elastic-wave velocities. Moreover, it will be shown that this conclusion also relates to rocks, for which an additional, non-Biot and non-squirt dispersion mechanism was earlier [9] supposed.

2. Basic equations

In this section we briefly recall the main features of the effective medium model [10] describing the elasticity and wave dissipation in microheterogeneous solids (below the model will be used only in the elastic part). In the model, the material (rock) is considered as a solid matrix containing defects-inclusions (grains, cracks, etc.) that are isotropically-oriented and small compared to the length of elastic waves, the compliance of the defects being much higher compared to the surrounding defect-free material. The characteristic diameter of the defects and their separation are supposed to be much smaller than the elastic wave length. It is also assumed that the concentration of the defects is small, so that their interaction can be neglected. In principle, the interaction effect could be additionally introduced in the model using, for example, a kind of "self-consistent approximation" similar to that used in [13]. However, the main purpose of model [10] was not the investigation of its ultimate possibilities to describe materials with high defect concentrations, but instructive elucidation of differences in the influence of defects with different ratios of normal-to-shear compliances on elastic moduli (and dissipation) of elastic waves of different types. It will be shown below that, even if neglecting the interaction of the defects, model [10] describes quite satisfactorily the defect-induced reduction in the elastic wave velocities by 20–30 % compared to their ultimate ("matrix") values corresponding to maximum confining pressures at which the crack-like defects in the samples are practically closed.

In order to quantitatively characterize compliance of planar defects in response to normal stress σ_n and to shear stress σ_τ in the in-plane direction, small parameters $\varsigma \ll 1$, $\varsigma \in [0, 1]$ and $\xi \ll 1$, $\xi \in [0, 1]$ were introduced in model [10]. These parameters relate Young's modulus E and shear modulus G for the matrix material with the effective moduli E_d and G_d of the defects:

$$E_d \equiv \varsigma E, \quad G_d \equiv \xi G. \tag{1}$$

Parameters ς and ξ thus are close to the nondimensional weaknesses used in [20, 21]. The orientation of the defects with different compliances is characterized by a distribution function $\nu(\psi, \varphi, \varsigma, \xi)$ that depends on both the orientation angles ψ, φ of the defect normal vector and the non-dimensional elastic parameters ς, ξ. For the isotropic orientation, the angular part of the distribution is $\nu(\psi, \varphi) = 1/(4\pi)$. Summation over all orientations and compliances gives the total volume content of the planar defects in the unit volume of the material

$$\nu_t = \int_0^{2\pi} d\varphi \int_0^{\pi} \int_0^1 \int_0^1 \nu(\psi, \varphi, \varsigma, \xi) \sin\psi \, d\psi d\varsigma d\xi,$$

which is much smaller than unity, according to the assumption that the characteristic distance between the defects is much smaller than their size.

Considering the amounts of the elastic energy stored in the matrix material and at the compliant defects and performing statistical averaging, we obtained the following expressions for the bulk modulus K_{eff}, the Young modulus E_{eff}, the shear modulus G_{eff}, modulus M_{eff} for the longitudinal (compressional) wave and Poisson's ratio γ_{eff} in the microheterogeneous material [10]:

$$\widetilde{K} = \frac{K_{\text{eff}}}{K} = \frac{1}{1 + \frac{1}{3} N_1/(1-2\gamma)}, \tag{2}$$

$$\widetilde{E} = \frac{E_{\text{eff}}}{E} = \frac{1}{1 + \frac{1}{5} N_1 + \frac{4}{15}(1+\gamma) N_2}, \tag{3}$$

$$\widetilde{G} = \frac{G_{\text{eff}}}{G} = \frac{1}{1 + \frac{2}{15} N_1/(1+\gamma) + \frac{2}{5} N_2}, \tag{4}$$

$$\widetilde{M} = \frac{M_{\text{eff}}}{M} =$$

$$= \frac{1 + \frac{4}{15} N_1/(1-\gamma) + \frac{2}{15} N_2 (1+\gamma)/(1-\gamma)}{\left[1 + \frac{2}{15} N_1/(1+\gamma) + \frac{2}{5} N_2\right]\left[1 + \frac{1}{3} N_1/(1-2\gamma)\right]}, \tag{5}$$

$$\gamma_{\text{eff}} = \frac{\gamma - \frac{1}{15} N_1 + \frac{2}{15}(1+\gamma) N_2}{1 + \frac{1}{5} N_1 + \frac{4}{15}(1+\gamma) N_2}. \tag{6}$$

Here notations E, G, and M relate to the moduli for the host material and $\widetilde{E}$, $\widetilde{G}$, and $\widetilde{M}$ are the corresponding non-dimensional moduli for the microheterogeneous medium. Parameters N_1 and N_2 in expressions (2)–(6) in the quasi-static limit (neglecting the defect relaxation) have the following meaning:

$$N_1 = \int \nu(\varsigma) \varsigma^{-1} d\varsigma, \quad N_2 = \int \nu(\xi) \xi^{-1} d\xi, \tag{7}$$

where partial distributions over parameters ς, ξ are introduced:

$$\nu(\varsigma) = \int_0^{2\pi} d\varphi \int_0^{\pi} \int_0^1 \nu(\psi, \varphi, \varsigma, \xi) \sin\psi d\psi d\xi,$$

$$\nu(\xi) = \int_0^{2\pi} d\varphi \int_0^{\pi} \int_0^1 \nu(\psi, \varphi, \varsigma, \xi) \sin\psi d\psi d\varsigma. \tag{8}$$

Below parameters N_1 and N_2 are called the effective normal and shear densities of the defects, respectively. It is clear from equations (7), that these parameters are determined jointly by the compliance of the defects and their concentration. In the case of identical defects with fixed values of ς and ξ, the distributions have the form of delta-functions, so that

$$N_1 = \nu_t/\varsigma, \quad N_2 = \nu_t/\xi$$

and effective densities N_1 and N_2 are proportional to the defect volume content divided by the compliance parameters.

Note that expressions (2)–(6) in the case of small concentration of the defects are similar to the equations derived in [13] using the "self-consistent" approximation, however, in [13] the contributions of the normal and shear compliances of the cracks were not explicitly singled out.

In the next section, Eqs. (2)–(6) will be used for determining the ratios of the normal-to-shear compliances of real defects by examination of known experimental data on pressure-dependencies of elastic waves.

3. Comparison between the model and experimental data

In this section, we use an instructive set of experimental data on elastic P- and S-wave velocities versus confining pressure, which were discussed in [8, 9] for sandstones typical of oil reservoirs. In papers [8, 9] applicability of the squirt mechanism to interpretation of the observed dependencies for elastic P- and S-waves was discussed in details. The purpose of the below examination is to evaluate the above introduced normal and shear compliance parameters N_1, N_2 and to determine the average ratio N_1/N_2 for the defects in the rock samples. According to equations (2)–(6), for this purpose it is necessary to know experimentally measured velocities (or elastic moduli) for two different types of waves in the rock with the defects. As the reference values for the matrix rock, following [9], we shall take the ultimate velocities measured at the highest hydrostatic pressures (50–100 MPa). Note that at such pressure, the "matrix" elasticity may still be affected by weakly compliant spheroidal and near-cylinder pores (equant porosity), whose contribution is dominant in the overall porosity (about 9–12 %) of the samples [8, 9]. It was noted in [8] that, in the considered pressure-range, the variation of the equant porosity was yet very small, so that the observed pronounced variations of the velocities were predominantly due to the effect of high-compliance planar fractures. The negligible variation in the total porosity allowed us to neglect the variation in the material density attributing the variation in the velocities only to the change in the elastic moduli.

For comparison of the observed and predicted velocity variations, it is convenient to present the data on the velocity pressure dependencies in the form of a plot of the relative variations $\Delta V_S/V_S$ in the S-wave velocity against the variations $\Delta V_P/V_P$ in the velocity of the P-wave. The variations ΔV_S and ΔV_P are counted from the ultimate high-pressure ("matrix") values. Figure 1 presents a set of such theoretically modeled dependencies plotted for different ratios

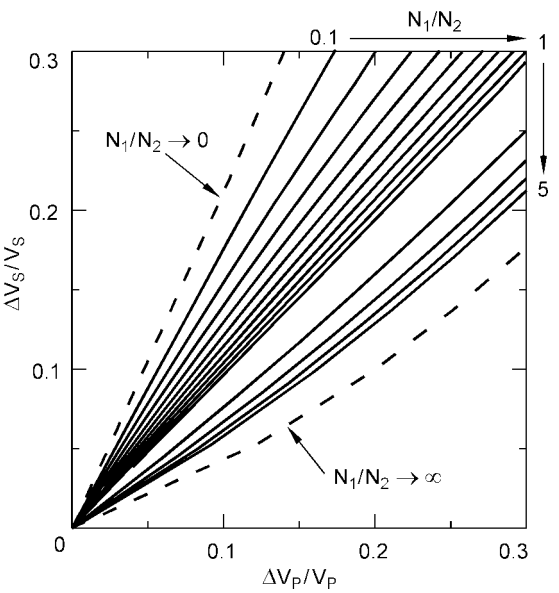

Fig. 1. Example of a plot demonstrating sensitivity of the complementary velocity variations to the defect properties. Ratio N_1/N_2 ranges from 0.1 to 1 (step 0.1) and from 1 to 5 (step 1). Dashed lines are for the ultimate cases $N_1/N_2 \to 0$ and $N_1/N_2 \to \infty$

N_1/N_2 using Eqs. (4) and (5). The plot instructively demonstrates the sensitivity of the defect-induced variations in the velocities to the variation in ratio N_1/N_2. For the whole range $0 \le N_1/N_2 < \infty$ of the defect compliance ratio, the resultant complementary variations in P- and S-velocities are confined within a rather narrow sector enclosed between the dashed lines corresponding to the ultimate cases $N_1/N_2 = 0$ (normal compliance is negligibly small) and $N_1/N_2 \to \infty$ (shear compliance is negligibly small).

Considering Fig. 1 one may pose a question, which pair of the velocities or elastic parameters should be plotted one against another in order to get the maximum sensitivity of the plot to variations in the compliance ratio N_1/N_2 for the defects? An evident answer is to choose such combinations of the moduli that are equal to the introduced "normal-" and "shear densities" N_1 and N_2. Such a plot on the plane (N_1, N_2), besides the relative parameter N_1/N_2, directly shows the effective defect densities $N_{1,2}$, whereas the sector of the allowable variations (see Fig. 1) transforms into the whole quadrant. Equations (2)–(5) readily yield for the parameters $N_{1,2}$ the required combinations of the elastic moduli:

$$N_1 = 3(K_m/K - 1)(1 - 2\gamma), \tag{9}$$

$$N_2 = (5/2)(G_m/G - 1) - \\ -(K_m/K - 1)(1 - 2\gamma)/(1 + \gamma). \tag{10}$$

Result (9) is intuitively quite clear. Indeed, the bulk elastic modulus is sensitive only to the normal (compressional) compliance of the defects. However, combination (10), which is sensitive only to the shear compliance of the defects, is not so obvious and it could be readily found just due to explicit singling out of contributions of the shear and normal compliances of the defects in Eqs. (2)–(6). Below we shall use both the plot of $\Delta V_S/V_S$ versus $\Delta V_P/V_P$, and the plot on the plane (N_1, N_2) using Eqs. (9)–(10) and known expressions relating modulus K with moduli G and M for S- and P-waves.

Following paper [9], consider the first experimental example for the Navajo sandstone (data obtained in [25]). In Fig. 2(*a*) the raw experimental points for the velocities are re-plotted in terms of $\Delta V_S/V_S$ and $\Delta V_P/V_P$, and are fitted by the theoretical curves based on Eqs. (4) and (5). The fit for the dry rock corresponds to the compliance ratio $N_1/N_2 \approx 2.35$, which is fairly close to the value $N_1/N_2 = (1+\gamma)(2-\gamma) \sim 2$ expected for elliptical cracks. For the saturated rock, this ratio is almost 3 times smaller, $N_1/N_2 \approx 0.8$, which is yet close to unity, but is not nearly zero in contrast to conventional assumptions for fully-saturated rocks [13, 20, 21]. This rather high residual normal compliance of the saturated defects indicates that, in the elastic wave field, the weakly compressible liquid is not "locked" inside the defects, but squirts forth and back in narrow compliant pores in agreement with the local-flow concept.

Another remarkable feature of Fig. 2(*a*) is that the experimental data are well fitted by the theoretical curves corresponding to constant values of the ratio N_1/N_2 in the whole pressure range, which is not an a priori evident property. Figure 2(*b*) additionally indicates that at zero pressure (when the defects are maximally opened) the effective "shear density" N_2 of the defects remains approximately the same for the dry and saturated Navajo sample. In contrast, the "normal density" N_1 for the saturated rock decreases roughly three times due to the presence of liquid in the defects.

The next plot in Fig. 3 (*a*) is presented in the form similar to that used in paper [9] and shows the experimental pressure dependencies of the wave velocities together with the theoretical curves corresponding to the above inferred values of N_1/N_2. Certainly expressions (2)–(6) do not determine explicitly the pressure-dependence for N_1 and N_2. In view of this in order to plot the theoretical curves in Fig. 3 (*a*) starting from the plots on the plane $(\Delta V_P/V_P, \Delta V_S/V_S)$, we had to use the experimentally determined high-pressure values for the "matrix" velocities and the pressure-dependence of the velocity for one of the two waves. Then for the other wave the expected values of the velocity were calculated for the chosen ratio N_1/N_2. In the form shown in Fig. 3(*a*) the deviations between the measurement data and the resultant theoretical fits are hardly distinguishable. Note that a similar procedure was actually used in [9] for plotting analogous theoretical curves for the two waves. In the procedure, the pressure dependencies for the dry samples were taken as reference data and then the expected variations in

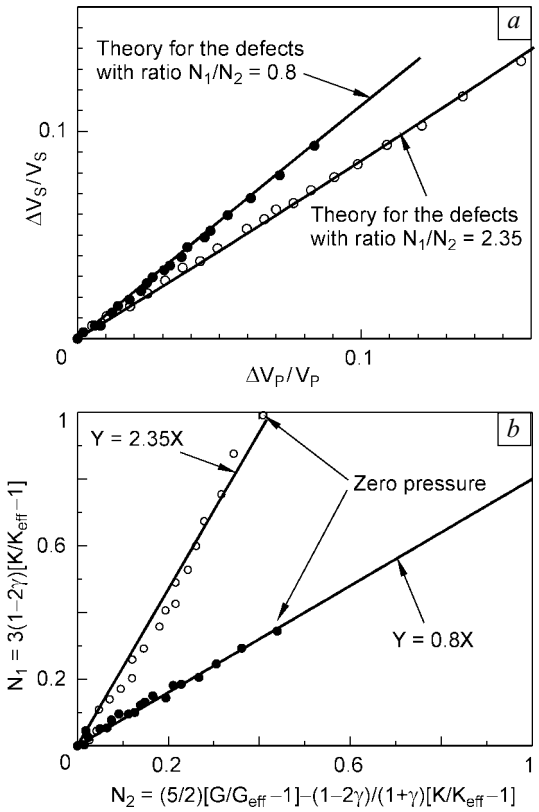

Fig. 2. Experimental points for the Navajo sandstone (data from [25]) plotted on the plane $\Delta V_S/V_S$ against $\Delta V_P/V_P$ (*a*) and the effective "normal density" N_1 against "shear density" N_2 (*b*) on the plane (N_1, N_2). Empty symbols are for the dry sample, and the filled ones are for the saturated rock. Solid lines are the theoretical fits for $N_1/N_2 = 2.35$ (dry) and $N_1/N_2 = 0.8$ (saturated sample)

the velocities for the saturated samples were added to the reference values. An example of the curves obtained via this procedure is shown in the inset in Fig. 3(*a*). This plot indicates that the corrections calculated using the Gassman and Biot models (that is taking into account the saturation of the equant porosity) do strongly deviate from the experimental data for the saturated sample. The improved model by the authors of paper [9] (curve marked by initials M-J) demonstrates noticeably better results, although the deviation of the improved curve from the experiment is still rather noticeable (compare with the perfect coincidence of the experimental points and the fits in Fig. 3(*a*)). The reasons of the discrepancy noted in [9] will be elucidated below after examination of some other examples. In conclusion of the discussion of the Navajo sample, in the next Fig. 3(*b*) the dependencies taken from Fig. 3(*a*) are re-plotted in terms of the pressure dependence of Poisson's ratio. In Fig. 3(*b*), although the coincidence with the fits is very good, minor systematic deviations between the theoretical curve and the measurements become noticeable for the dry rock (which could not be distinguished in Fig. 3(*a*)). Qualitatively the illustrated in Fig. 3(*b*) decrease of Poisson's ratio with increased density of the dry defects (and, in contrast, the Poisson ratio growth for the increased concentration of saturated defects) agree well with known theoretical predictions (see, for example, [13]). However, in [13] it was predicted that, at high enough density of the defects, Poisson's ratio should become zero together with all elastic moduli, which may be interpreted as complete fracture of the material. The following example demonstrates that the real situation may be essentially different.

Following further paper [9], consider the Weber sandstone as the next sample. The respective experimental data (obtained in [25]) are re-plotted in Fig. 4 on the planes $(\Delta V_P/V_P, \Delta V_S/V_S)$ and (N_1, N_2) together with the theoretical fits. Figure 4(*b*) indicates that the effective "shear density" N_2 at zero pressure for the Weber sandstone remains practically the same in the dry and saturated states, much like in the case of the Navajo sandstone. However, for the

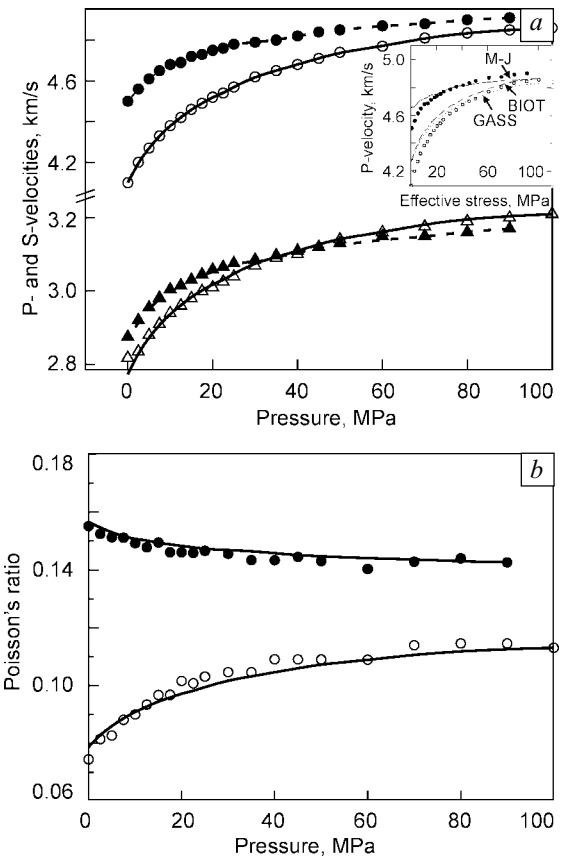

Fig. 3. Pressure dependencies for the Navajo sandstone (data from [25]) plotted for the wave velocities (*a*) and for the Poisson ratio (*b*). Empty symbols are for the dry sample, filled symbols are for the saturated rock. In plot (*a*) triangles are for the S-wave, circles are for the P-wave. Lines are the theoretical fits for $N_1/N_2 = 2.35$ (dry) and $N_1/N_2 = 0.8$ (saturated sample). In the inset for comparison the same experimental data for the P-wave and superimposed model curves are reproduced from paper [9]

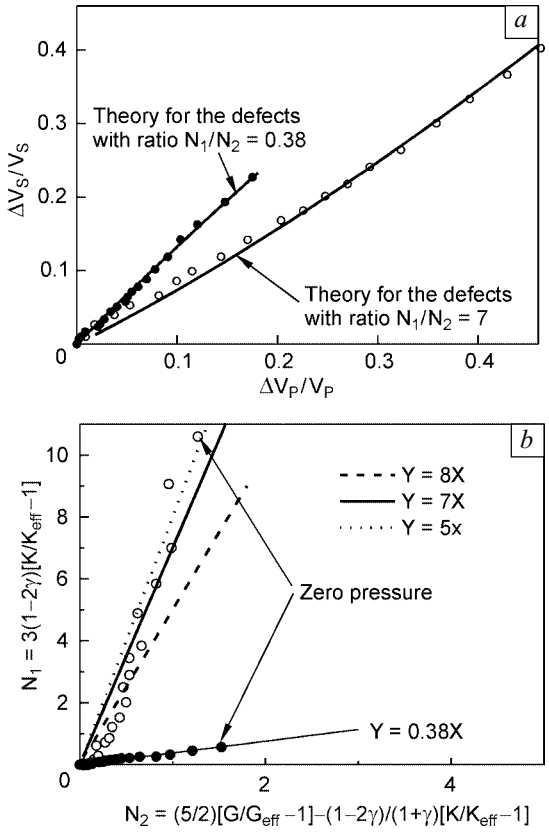

Fig. 4. Experimental points for the Weber sandstone (data from [25]) plotted on the plane $\Delta V_S/V_S$ against $\Delta V_P/V_P$ (*a*) and the effective "normal density" N_1 against "shear density" N_2 (*b*) on the plane (N_1, N_2). Empty symbols are for the dry sample, and the filled ones are for the saturated rock. Solid lines are the theoretical fits for $N_1/N_2 = 7$ (dry) and $N_1/N_2 = 0.38$ (saturated sample)

Weber sandstone in the saturated state the ratio of the normal to shear compliance is reduced stronger than in the Navajo sandstone, from $N_1/N_2 \sim 7$ down to $N_1/N_2 = 0.38$. The difference thus is almost 20 times in contrast to 3 time difference for the Navajo sample. Furthermore, for the dry Weber sample the estimated ratio $N_1/N_2 \sim 7$ is significantly higher than that expected for such basic models of the defects as elliptical cracks or Hertz-Mindlin contacts. More detailed examination of Fig. 4(*b*) indicates that the estimate of N_1/N_2 at different pressures exhibits noticeable variability in the range 5–8. The reason for this may be both the actual variability of the defect parameters and the neglect of the defect interaction in the theoretical description (note that the pressure-induced variations in the velocities reached 20–25 % for the saturated sample and over 40 % for the dry one). However, even the mean constant value $N_1/N_2 = 7$ provides a very good theoretical fit for the velocity variations in the whole pressure range, which is shown in Figs. 4(*a*) and 5(*a*).

Finally, Figure 5(*b*) presents the pressure dependence of the Poisson ratio for the Weber sandstone. The most remarkable feature of this plot is the pronounced negative value of Poisson's ratio for the dry sample at pressures below 20 MPa, at which the wave velocities are only 25 % reduced compared to the high-pressure values. This fact contrasts with the above mentioned model [13], which predicts that the material should become completely fractured when Poisson's ratio reaches zero. It should be stressed specially that the character of the relation between the elastic moduli in the Weber sample indicates that the material is isotropic with a good accuracy.

Physically the origin of the negative Poisson ratio in crack-containing materials may be readily understood. Let us assume first that the compliant planar defects had no shear compliance at all (that is for them $N_1/N_2 \to \infty$). If such defects were all oriented at 45 degrees to the direction of the uniaxial stress, then such defects should produce equal additional expansions of the same sign both in the direction of the applied stress and in the orthogonal direction. At high enough density of such soft defects the contribution of the solid matrix to the overall strain could be neglected, so that the effective (and essentially anisotropic) Poisson's ratio should tend to minus unity. Certainly for isotropically oriented defects their averaged additional contribution to the material expansion should be smaller (but still keep the same sign for the along-stress and normal directions). Besides, real defects had a non-zero shear compliance, which additionally diminishes their reducing effect on the Poisson ratio (see Eq. (6)). In the isotropic case the expression for ultimate minimum Poisson's ratio for a fixed value $N_1/N_2 \neq 0$ follows from Eq. (6) at very high "normal density" N_1:

$$\gamma_{\min} = \frac{-1 + 2(1+\gamma)\, N_2/N_1}{3 + 4(1+\gamma)\, N_2/N_1}.$$

This expression yields $\gamma_{\min} = -1/3$ for the defects without shear compliance at all $(N_2/N_1 \to 0)$. For the Weber sandstone with $N_1/N_2 \approx 7$ we obtain the estimate $\gamma_{\min} \approx -0.19$, so that the experimental minimum $\gamma_{\text{eff}} \approx -0.13$ is not so far from the theoretical limit. The transition from the negative to positive values of the Poisson ratio is fairly well described by the theoretical curve (see Fig. 5(*b*)) based on equations (2)–(6), which may be ever improved using a kind of self-consistent approximation in order to accounting for interaction of the defects.

The next Figures 6 and 7 present the results for the Nugget V sandstone (data obtained in [26]), for which in paper [9] an unidentified dispersion mechanism was supposed different from the Biot- and squirt-mechanisms. The theoretical fits in Fig. 6 indicate that for the saturated Nugget sample the defect compliance ratio is very close to that for the Weber sandstone, $N_1/N_2 \approx 0.38$, whereas for the dry defects this ratio is $N_1/N_2 \approx 4.3$, being intermediate between the values determined for the Navajo and Weber samples. The Poisson coefficient for the dry Nugget sandstone

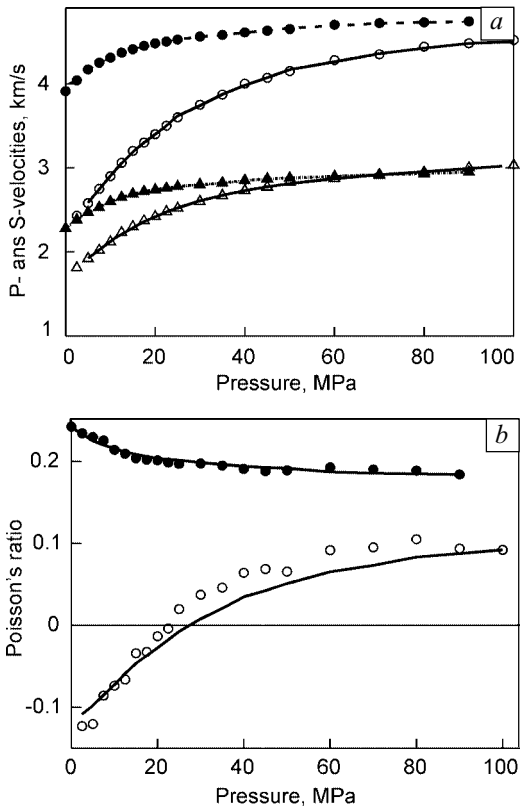

Fig. 5. Pressure dependencies for the Weber sandstone (data from [25]) plotted for the wave velocities (*a*) and for the Poisson ratio (*b*). Empty symbols are for the dry sample, filled symbols are for the saturated rock. In plot (*a*) triangles are for the S-wave, circles are for the P-wave. Lines are the theoretical fits for $N_1/N_2 = 7$ (dry) and $N_1/N_2 = 0.38$ (saturated sample). At pressures below 20 MPa the Poisson ratio for the dry sample is negative

is strongly reduced (down to 0.03), but because of smaller density of the defects compared to the Weber sample (compare Figs. 6(*b*) and 4(*b*)) the negative region is not yet reached for the Nugget sandstone. The most remarkable feature of the latter sample, which is visible in Fig. 6(*b*), is that the effective shear density N_2 at zero pressure in the saturated Nugget V sample is significantly higher than that in the dry rock. This fact differs significantly from a practically constant analogous value N_2 for the first two samples in both dry and saturated states (compare Fig. 6(*b*) with Figs. 2(*b*) and 4(*b*)). For the right experimental points in Fig. 6(*b*) (corresponding to zero applied pressure) it is clearly seen that in the Nugget sandstone the parameter N_2 increases more than $0.6/0.4 = 1.5$ times for the saturated state of the rock compared to the dry state. Thus the presence of liquid results in enhancement of the defect shear compliance in the case of the Nugget sample

The plots for the velocities shown in the next Fig. 7(*a*) for the Nugget sample indicate that even at highest pressures this additional shear compliance of the saturated defects persists, so that the S-wave velocity in the saturated sample is noticeably less than in the dry rock. In contrast, for the Navajo and Weber sandstones the high-pressure wave-velocities became almost equal in the dry and saturated cases. When these "background" variations in the high-pressure wave velocities are taken into account, then the complementary pressure dependencies of the P- and S-wave velocities are perfectly approximated by the fits based on model [10]. The next Fig. 7(*b*) displays the pressure dependence for the Poisson ratio in the Nugget sandstone and also demonstrates a perfect agreement with the theoretical fits for both the dry and saturated Nugget samples. Importantly that the influence of saturation is accounted in model [10] only via the variation of the compliance ratio N_1/N_2 for the high-compliant crack-like porosity due to presence of liquid. This indicates that the role of the local squirt-type flows inside the high-compliant defects is dominant in the pressure-dependent wave dispersion. The latter conclusion relates to all the considered examples including the Nugget sandstone and similar rocks, for which the interpretation used in papers [8, 9] apparently indicated the presence of some unidentified, non-Biot and non-squirt mechanism.

The analysis performed provides an explanation for this apparent discrepancy mentioned in paper [9], in which the authors used in their interpretation some expected relationship between the saturation-induced complementary variations of different elastic moduli. Equations (2)–(6) allow one to clearly see both the difference and similarity with interpretation [9]. This interpretation was based on the derived in [8] relation between the dispersion corrections to the bulk elastic modulus and the shear modulus for a solid with defects:

$$\left(\frac{1}{G_{\rm uf}} - \frac{1}{G_{\rm dry}}\right)_\sigma \approx \frac{4}{15}\left(\frac{1}{K_{\rm uf}} - \frac{1}{K_{\rm dry}}\right)_\sigma, \qquad (11)$$

where index "uf" denotes the unrelaxed (high-frequency) value of the respective modulus, and index "dry" corresponds to the relaxed (low-frequency) moduli. Physically these frequency-dependent variations of the moduli occur, since the compliance of the defects can be different at different frequencies. Similar to [8, 9] in Eqs. (2)–(6), where the compliance parameters $N_{1,2}$ are not predetermined, one may consider that variations $\Delta N_{1,2}$ of the effective densities depend not only on the confining pressure and fluid saturation, but on frequency as well. Thus the resultant complementary variations in the elastic moduli $\Delta(1/G_{\rm eff})$ and $\Delta(1/K_{\rm eff})$ caused by any of the mentioned factors can be compared with each other. Similar logical conclusions were used in [8, 9] for the transition from Eq. (11) describing the frequency-dependent variations of the moduli to the variations caused by the pressure variation and fluid saturation. Namely, the complementary variations of moduli $G_{\rm eff}$ and $K_{\rm eff}$ of the saturated materials were found in [9] by substi-

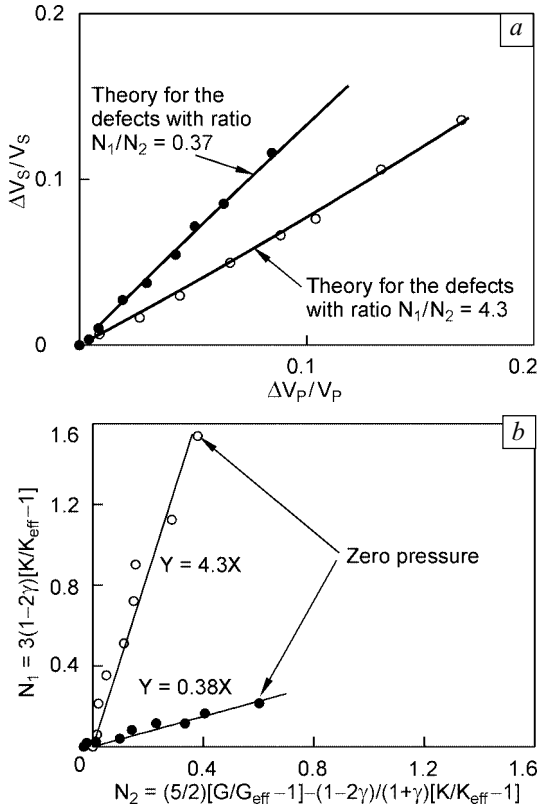

Fig. 6. Experimental points for the Nugget V sandstone (data from [26]) plotted on the plane $\Delta V_S/V_S$ against $\Delta V_P/V_P$ (*a*) and the effective "normal density" N_1 against "shear density" N_2 (*b*) on the plane (N_1, N_2). Empty symbols are for the dry sample, and the filled ones are for the saturated rock. Solid lines are the theoretical fits for $N_1/N_2 = 4.3$ (dry) and $N_1/N_2 = 0.38$ (saturated sample)

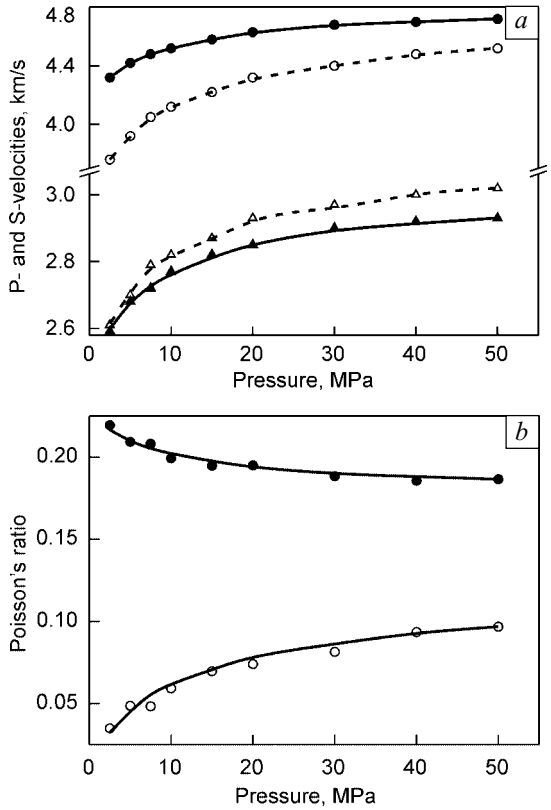

Fig. 7. Pressure dependencies for the Nugget V sandstone (data from [26]) plotted for the wave velocities (*a*) and for the Poisson ratio (*b*). Empty symbols are for the dry sample, filled symbols are for the saturated rock. In plot (*a*) triangles are for the S-wave, circles are for the P-wave. Lines are the theoretical fits for $N_1/N_2 = 4.3$ (dry) and $N_1/N_2 = 0.38$ (saturated sample)

tuting Eq. (11) into the low-frequency Biot–Gassman equations, which yielded approximately:

$$\left(\frac{1}{G_{\text{sat}}}-\frac{1}{G_{\text{dry}}}\right)_{\sigma} \approx$$

$$\approx \frac{4}{15}\left[\left(\frac{1}{K_{\text{sat}}}-\frac{1}{K_{\text{dry}}}\right)_{\sigma}-\left(\frac{1}{K_{\text{sat}}}-\frac{1}{K_{\text{dry}}}\right)_{\text{high}\sigma}\right]. \qquad (12)$$

Index "σ" in (12) is for the current pressure, whereas "high σ" corresponds to the maximum pressure on the sample (when the compliant defects are closed). Indices "sat" and "dry" correspond to the saturated and dry states of the material, respectively. Relations (11), (12) were used in [9] as criteria of the domination of the squirt-flow mechanism when examining experimental data. Note that factor 4/15 in Eqs. (11), (12) is of geometrical nature and originates due to averaging over random orientations of the defects, much like the similar factors in our Eqs. (2)–(6). Comparison between Eqs. (2), (4) and (11), (12) indicates that Eqs. (2) and (4) yield the following analog of Eqs. (11), (12):

$$\Delta\left(\frac{1}{G_{\text{eff}}}\right) \approx \frac{4}{15}\Delta\left(\frac{1}{K_{\text{eff}}}\right)+\frac{2}{5}\frac{1}{G}\Delta N_2. \qquad (13)$$

In the derivation of (13) the known relation $G = (3/2)K(1-2\gamma)/(1+\gamma)$ was used. Since the bulk modulus K_{eff} is not sensitive to the variation of the shear density of the defects, the variation N_2 is present in the right hand side of Eq. (13) independently of the variations of K_{eff}. Expression (11) agrees with (13) if in the right hand side of the latter it is possible to neglect the second term or, in other words, to neglect the contribution of the shear density N_2 to the variation of the shear modulus G_{eff}. Equation (4) indicates that this contribution can be neglected under a rather strict condition on the compliance ratio $N_1/N_2 \gg \gg 3(1+\gamma) > 3$. As it was shown above, for the considered samples (intentionally chosen exactly the same as in [9]) this ratio appeared to fall in the range $N_1/N_2 \approx 2$–7 for the dry defects and $N_1/N_2 < 1$ for the saturated ones. Therefore, even for the dry samples exhibiting ratio $N_1/N_2 > 1$ the assumption $N_1/N_2 \gg 3(1+\gamma)$ is rather poor in most cases, not saying about saturated samples with $N_1/N_2 < 1$.

Concerning the second relation (12), which was used in [9] as the main criterion of the squirt-mechanism domination in the course of the comparison between the dry and saturated samples, actually this criterion requires significantly softer restrictions than Eq. (11), so that assumption $N_1/N_2 \gg \gg 3(1+\gamma)$ is not necessary. Namely, Eq. (12) with the proportionality coefficient 4/15 may be readily obtained from Eqs. (2), (4) and (13) in the assumption that fluid saturation does not affect the shear compliance N_2 of the defects. Thus criterion (12) implies that the difference between values G_{sat} and G_{dry} is determined, in our terms, exclusively by the pressure- and saturation-dependent variation in "normal density" N_1 corresponding to the normal compliance of the soft porosity. Therefore, possible "background" variation of the shear modulus (e.g. related to variation of N_1 due to the weakly compliant equant porosity in the whole range of pressure) as well as the variation in the shear parameter N_2 due to saturation are not taken into account in the left hand side of criterion (12). In contrast, in the right hand side of Eq. (12), which in our terms depends only on the normal density N_1, the second term in the parentheses subtracts the "background" variation in the bulk modulus *K*, which has been neglected for the shear modulus. Therefore, the initial assumptions accepted in the derivation of Eq. (12) strictly speaking are not consistent with each other and do not take into account possible "background" variation of the shear density N_2. The validity of relation (12) thus may be broken for samples in which fluid saturation noticeably affects the shear parameter N_2.

The experimental pressure dependencies of S-wave velocity shown in Fig. 3(*a*) and 5(*a*) together with the plots on the plane (N_1, N_2) shown in Figs. 2(*b*), 4(*b*) indicate that the assumption on the same shear parameter N_2 in the dry and saturated states holds quite well for the Navajo and Weber sandstones. This fact explains a good agreement with criterion (12), which was mentioned in [9] for those and similar samples. On the other hand, for the Nugget sandstone Figure 7(*a*) indicates rather significant "background" (high-pressure) variations both for the P- and S-wave velocities. This pronounced "background" variation in the shear modulus *G* due to the aforementioned strong increase of the defect shear compliance N_2 in the saturated Nugget sandstone (see Fig. 6(*b*)), which was not taken into account in Eq. (12), resulted in bad agreement with criterion (12). The latter fact was interpreted in [9] as the manifestation of some unidentified dispersion mechanism.

On the other hand, in Eqs. (2)–(6) and in the theoretical curves shown in Fig. 7 such "background" variations are consistently taken into account for both moduli *K* and *G*, so that for the Nugget sample the pressure-dependent part of the wave dispersion is also very well fitted by the theoretical curves that account only for the compliance properties of the high-compliant porosity (including the saturated case). This is equivalent to taking into account only the squirt-flows inside the compliant defects.

Here we limit ourselves to the considered instructive examples, which we intentionally took exactly the same as in paper [9] for the convenience of the comparison. A number of other examined experimental records taken from [8, 9, 27, 28] also exhibited very similar features and all were well fitted by Eqs. (2)–(6) with a high accuracy. Thus in all considered cases the pressure-dependent experimental data are described very well by the model accounting only for the effect of the high-compliant porosity, which corresponds to accounting for the squirt-flows only for the saturated samples. It may be noted that for all law-porosity samples studied in [28] the determined compliance ratio N_1/N_2 appeared to be close to two, which is typical of the elliptical crack model.

4. Conclusions

The analysis performed has led us to a number of inferences, which are important for understanding of the relation between seismic waves parameters and the microstructure of rocks. The main conclusion may be summarized as follows.

Concerning the relation between P- and S-wave velocities the examination performed indicates that the effective medium model [10] allows for description of the complementary variations in the velocities of different types of waves for both dry and saturated rocks. The procedure of the performed examination may be considered as a development of the approach used in paper [9]. The results of the modified interpretation indicate strong domination of the squirt-flow mechanism in the observed complementary pressure variations in the elastic moduli for the saturated samples. This conclusion is shown to be valid even for those cases, for which earlier [9] an unidentified non-squirt and non-Biot mechanism was supposed.

The suggested approach allowed us to estimate the ratio N_1/N_2 of the normal to shear compliances for real defects, as well as the effective defect densities $N_{1,2}$ themselves. The performed examination indicated a number of unexpected results. Namely, for some dry samples, the compliance ratio N_1/N_2 was found to be much greater than unity (e.g., $N_1/N_2 \approx 7$ for Weber and $N_1/N_2 \approx 4.3$ for the Nugget V sandstones) in contrast to conventionally expected for this ratio value about unity [13, 16, 21]. Such a high normal compliance of real defects may result in negative values of Poisson's ratio, which we have found for the dry Weber sandstone at confining pressures below 20 MPa.

On the other hand, for the saturated samples, instead of the conventionally expected almost zero compliance ratio [13, 21] we have found values of N_1/N_2 of the order of unity (for example, $N_1/N_2 \approx 0.8$ for the saturated Navajo sandstone). These findings are important for discrimination of dry and saturated rocks using seismic data.

Another important and not evident a priori inference is that in all examined cases the compliance ratio N_1/N_2 for the defects persistently keeps constant value in a wide pres-

sure range, up to the maximum pressures corresponding to almost complete closing of the compliant defects. The performed examination has proved that model [10] describes the microstructure-induced variations in the elasticity with quite a good accuracy, including the influence of saturation of the microstructural defect. The revealed features of the rocks should be taken into account in planning optimal seismo-prospecting and in interpretation of the obtained seismic data.

The study was partially supported by the RFBF (Project No. 02-02-16237) and by a project "Neue Hochleistungswerkstoffe fur effiziente Energienutzung" at the University of Saarbruecken (V.Z.). We thank Prof. S. Shapiro and Dr. A. van der Kallen for stimulating discussions.

References

[1] T. Bourbie, O. Coussy, and B. Zinszner, Acoustics of Porous Media, 1987, A.A. Balkema.
[2] M.A. Biot, Theory of acoustic attenuation, propagation of elastic waves in a fluid-saturated porous solid: I. Low-frequency range, J. Acoust. Soc. Amer., 28 (1956) 168.
[3] M.A. Biot, Theory of propagation of elastic waves in a fluid-saturated porous solid: II. Higher frequency range, J. Acoust. Soc. Amer., 28 (1956) 179.
[4] G. Mavko, and A. Nur, Melt squirt in the asthenosphere, J. Geophys. Res., 80 (1975) 1444.
[5] W.F. Murphy, Acoustic measures of partial gas saturation in tight sandstones, J. Geophys. Res., 89 (1984) 11549.
[6] K.W. Winkler, Dispersion analysis of velocity and attenuation in Berea sandstone, J. Geophys. Res., 90 (1985) 6793.
[7] K.W. Winkler, Estimates of velocity dispersion between seismic and ultrasonic frequencies, Geophysics, 51 (1986) 183.
[8] G. Mavko and D. Jizba, Estimating grain-scale fluid effects on velocity dispersion in rocks, Geophysics, 56 (1991) 1940.
[9] G. Mavko and D. Jizba, The relation between seismic P- and S- velocity dispersion in saturated rocks, Geophysics, 59, No. 1 (1994) 87.
[10] V. Zaitsev and P. Sas, Elastic moduli and dissipative propertsies of microinhomogeneous solids with isotropically oriented defects, Acustica-Acta Acustica, 86 (2000) 216.
[11] J.B. 2000, The effect of cracks on the uniaxial elastic compression of rocks, J. Geoph. Res., 70 (1965) 399.
[12] J.B. Walsh, The effect of cracks on Poisson's ratio, J. Geoph. Res., 70 (1965) 5249.
[13]B. Budiansky and R.J. O'Connel, Elastic moduli of dry and saturated cracked solids, Int. J. Solid Structures, 12 (1976) 81.
[14] G.M. Mavko and A. Nur, The effect of nonelliptical cracks on the compressibility of rocks, J. Geoph. Research, 83 (1978) 4459.
[15] K.L. Johnson, Contact Mechanics, Cambridge University Press, Cambridge, United Kingdom, 1999.
[16] K.W. Winkler, Contact stiffness in granular porous materials: comparison between theory and experiment, Geophys. Res. Lett., 10, No. 11 (1983) 1073.
[17] P.J. Digby, The effective elastic moduli of porous granular rocks, J. Appl. Mech., 48 (1981) 803.
[18] M. Schoenberg and J. Douma, Elastic wave propagation in media with parallel fractures and aligned cracks, Geophys. Prospecting, 36 (1988) 571.
[19] M. Schoenberg and C. Sayers, Seismic anisotropy of fractured rock, Geophysics, 60 (1995) 204.
[20] A.V. Bakulin and L.A. Molotkov, Effective models of fractured and porous media, St. Petersburg Univ. Press (in Russian).
[21] A. Bakulin, V. Grechka, and I. Tsvankin, Estimation of fracture parameters from reflection seismic data. Pts. I–III: Geophysics, 65, No. 6 (2000) 1788.
[22] V.N. Kostychenko, G.G. Kocharyan, and D.V. Pavlov, Deformation characteristics of inter-block gaps of different scales, Phys. mesomech., 5, No. 5 (2002) 23.
[23] S.P. Tokmakova, Cuts with negative poisson's ratio in crystals, in nonlinear acoustics at the beginning of the 21st century, (ISNA-16), Eds. by. O.V. Rudenko and O.A. Sapozhnikov (Faculty of Physics, MSU, Moscow, 2002), 2, 669.
[24] V.E. Nazarov and A.M. Sutin, On Poisson's ratio of crack-containg solids, Akust. Zhurn., 41, No. 6 (1995) 932.
[25] K.B. Coyner, Effects of stress, pore pressure, and pore fluids on bulk strain, velocity, and permeability in rocks, Ph.D. Thesis, Massachusetts Institute of Technology (1984).
[26] D. Han, Effects of porosity and clay content on acoustic properties of sandstones and unconsolidated sediments, Ph.D. Dissertation, Stanford University (1986).
[27] R.B. Gordon and L.A. Davis, Velocity and attenuation of seismic waves in imperfectly elastic rock, Journ. Geoph. Res., 73, No. 12 (1968) 3917.
[28] U. Seipold, H.-J. Mueller, and P. Tuisku, Principle differences in the pressure dependence of thermal and elastic properties of crystalline rocks, Phys. Chem. Earth, 23 (1998) 357.